High pressure Raman study of layered $Mo_{0.5}W_{0.5}S_2$ ternary compound

2016 2D Mater. 3 025003

(http://iopscience.iop.org/2053-1583/3/2/025003)

2D Materials

PAPER

High pressure Raman study of layered $Mo_{0.5}W_{0.5}S_2$ ternary compound

RECEIVED
27 October 2015

REVISED
24 February 2016

ACCEPTED FOR PUBLICATION
24 February 2016

PUBLISHED
30 March 2016

Joon-Seok Kim[1,5], **Samuel T Moran**[1,2,5], **Avinash P Nayak**[1,5], **Shahar Pedahzur**[2], **Itzel Ruiz**[2], **Gabriela Ponce**[2], **Daniela Rodriguez**[2], **Joanna Henny**[2], **Jin Liu**[3], **Jung-Fu Lin**[3,4,6] **and Deji Akinwande**[1,2,6]

[1] Department of Electrical and Computer Engineering, The University of Texas at Austin, Austin, TX 78712, USA
[2] NASCENT NSF Engineering Research Center (ERC), Austin, TX 78758, USA
[3] Department of Geological Sciences, The University of Texas at Austin, Austin, TX 78712, USA
[4] Center for High Pressure Science & Technology Advanced Research (HPSTAR), Shanghai 201203, People's Republic of China
[5] These authors contributed equally to this work.
[6] Author to whom any correspondence should be addressed.

E-mail: afu@jsg.utexas.edu **and** deji@ece.utexas.edu

Keywords: 2D materials, transition-metal dichalcogenide, high pressure, diamond anvil cell, alloy

Supplementary material for this article is available online

Abstract

Ternary two-dimensional (2D) transition metal dichalcogenide compounds exhibit a tunable electronic structure allowing for control of the interlayer and the intralayer atomic displacement to efficiently tune their physical and electronic properties. Using a diamond anvil cell, hydrostatic pressure was applied to $Mo_{0.5}W_{0.5}S_2$ up to 40 GPa in order to study the optical phonon vibrational modes. Analysis of the high-pressure Raman spectra shows that the two in-plane E_{2g} modes resembling that of pristine MoS_2 and WS_2, as well as disorder-activated longitudinal acoustic phonon mode, are hardened and suppressed as pressure increases. The two A_{1g} modes of the ternary compound that resemble the A_{1g} modes of pristine MoS_2 and WS_2, displayed similar Raman shifts to the pristine compounds as pressure increases. A Raman peak at 470 cm^{-1} that is close to A_{1g} peaks emerges at ~8 GPa, which represents a disorder-activated pressure-induced out-of-plane Raman mode observed only in the ternary compound under high pressure. At pressures above ~30 GPa, a Raman peak at approximately 340 cm^{-1} is observed, signifying additional disorder-activated vibration mode. Our results reveal the enhanced interactions in the structural and vibrational behavior of the MoS_2 and WS_2 domains in the $Mo_{0.5}W_{0.5}S_2$ compound under hydrostatic pressure. These results could have implications in understanding the electronic, optical, and structural properties of the new 2D ternary compound materials under extreme mechanical conditions.

1. Introduction

Two-dimensional (2D) materials are considered to have remarkable potential for applications in future electrical and optoelectronic devices. From the advent of graphene [1], several 2D materials have been isolated, which have diverse properties including insulators like hexagonal boron nitride [2, 3], semiconductors such as the transition metal dichalcogenides (TMDs) [4] and other elemental atomic materials such as phosphorene and silicone [5, 6]. Of these materials, the semiconducting TMDs are of particular interest for their tunable mechanical and electronic properties [7, 8]. For several 2D materials, the electronic bandgap and lattice structure of the material is tunable by adjusting the number of layers [9–11], intercalation with foreign molecules [12–14], applied mechanical strain [15, 16], stacked out-of-plane heterostructures [17, 18], and in-plane 2D heterostructures [19, 20]. In the case of TMDs, further engineering their properties can be achieved by adjusting its metal and chalcogen atom contributions to form ternary compounds with different elements from the same element group [8, 21–24]. Only a few TMD ternary compounds have been synthesized so far [19, 22, 25–28]. These ternary 2D compounds exhibit different electronic properties depending on their compositions [8, 22–24, 29–31]. The properties of

these 2D materials can be further altered by strain [16, 32, 33], hydrostatic pressure [34–36], chemical doping, and intercalation [13, 37–39]. Here, we explore the hydrostatic effects on multilayered $Mo_{0.5}W_{0.5}S_2$, an in-plane ternary compound, and elaborate on the comparative differences between the ternary compound and the pristine binary MoS_2 and WS_2 layered compounds.

2. Experimental

The $Mo_{1-x}W_xS_2$ ternary compound with $x = 0.5$ and purity 99.9995% was purchased from 2D semiconductors (SKU: BLK-MOWS2) and was used for the high-pressure diamond anvil cell (DAC) experiments. The FEI Quanta 650 scanning electron microscope (SEM) equipped with Bruker energy dispersive x-ray spectroscopy (EDX) system was used to analyze the chemical composition of the ternary compound. The JEOL 2010F transmission electron microscope (TEM) was used to evaluate the atomic crystal structure of the ternary compound. All Raman spectroscopy and photoluminescence (PL) measurements were done using the Renishaw InVia Raman system coupled with a continuous 532 nm green laser. The ruby PL (for *in situ* pressure determination) was measured using 0.000 001 mW for 1 s at a ~0.5 nm resolution with a grating of 1200 line mm^{-1}, while the Raman measurements were taken for 60 s for each given spectrum (6 accumulations of 10 s) with a laser power of 1 mW with ~1 cm^{-1} resolution at a grating of 3000 line mm^{-1}. These experimental settings as well as relative polarization of the incident light in the X direction were maintained throughout all measurements. The extreme hardness and optical transparency of the diamond anvils in a DAC, together with the use of a hydrostatic Ne pressure medium, allow for hydrostatic pressures to be exerted onto the sample, and offer *in situ* optical Raman measurements to be carried out up to the maximum pressure of 40 GPa in this study. An initially 250 μm thick Re gasket sheet was pre-indented using a pair of 350 μm diamonds and drilled in the middle of pre-indented area to form a sample chamber size of diameter 200 μm and thickness 40 μm. A $Mo_{0.5}W_{0.5}S_2$ ternary compound sample cleaved to size ~100 μm in diameter and ~10 μm in thickness was placed onto the very center of the sample chamber along with two pressure indicator ruby spheres (figure S1). Neon pressure medium gas was loaded into the sample chamber using the gas loading system; potential chemical reactions of the sample with pressure medium gas under high pressure was inhibited by use of inert Ne medium. Before loading gas, the sample chamber was vacuumed for 30 min to remove any potential water and volatile contamination in the sample.

3. Results and discussion

The isomorphism of TMD materials makes them great candidates to form ternary van der Waals (vdW) compounds. Two or more elements with similar properties can be alloyed into a new layered material, such as the $M_{0.5}W_{0.5}S_2$ ternary TMD (figure 1(a)). Characterizing the $Mo_{0.5}W_{0.5}S_2$ with SEM–EDX shows the elemental composition of the ternary TMD structure as well as the amounts of Mo, W, and S present in the sample (figure 1(b)); the uniformity of the EDX spectra indicates homogeneous chemical composition along the surface of the $Mo_{0.5}W_{0.5}S_2$ (figure S2). To further characterize the ternary compound, analysis of the TEM images shows the hexagonal lattice of the material, without any major disorder of the atomic structure (figure 1(c)). Although the chemical composition is static like that in the pristine MoS_2 or WS_2, slight difference in the lattice constants of the unit cell and arbitrary distribution of metal atoms might cause internal stress and local perturbation in vibrational modes. Previous studies on the Raman spectra of $Mo_{1-x}W_xS_2$ have reported a convolution of the two pristine Raman modes observed in MoS_2 and WS_2, but slight shifts of the peak positions are observed when the chemical composition of a given ternary compounds changes [23, 40]. These perturbations of the phonon modes suggest that distortion of the lattice constants and the disordered nature at the atomic scale have a large effect on the lattice and optoelectronic properties of the ternary compound material. Applying hydrostatic pressure onto the ternary compound can further distort the lattice structure and its electronic properties, and can be an effective means to investigate the optoelectronic and structural properties of the ternary TMDs under high strain conditions. Here, we apply hydrostatic pressure on the $Mo_{0.5}W_{0.5}S_2$ ternary compound to understand its lattice phonon vibrational behavior using Raman spectroscopy in a DAC.

For 2D materials, room temperature *in situ* micro-Raman spectroscopy has been used to study the effects of the number of layers [9, 22], unwanted byproducts [41], functional groups [42], structural damage [43], and chemical modifications [44]. Along with many other TMD materials, both 2H-MoS_2 and 2H-WS_2 exhibit D^4_{6h} symmetry (space group $P6_3/mmc$, No. 194) with specific Raman active phonon modes including out-of-plane A_{1g}, in-plane E^1_{2g}, rigid E^2_{2g}, and E_{1g} modes. We note that since E^2_{2g} rigid mode appears at ~35 cm^{-1} for MoS_2 and ~27 cm^{-1} for WS_2, respectively, which is below the cut-off frequency of the Raman system used in this study, and E_{1g} mode is only activated with specialized polarization environment, we restrict our analysis to A_{1g} and E^1_{2g} (noted as E_{2g} mode) modes in this study [45–47]. The convoluted Raman peaks for the $Mo_{0.5}W_{0.5}S_2$ compound clearly shows the two in-plane E_{2g} modes from pristine MoS_2 and WS_2, and the two A_{1g} modes

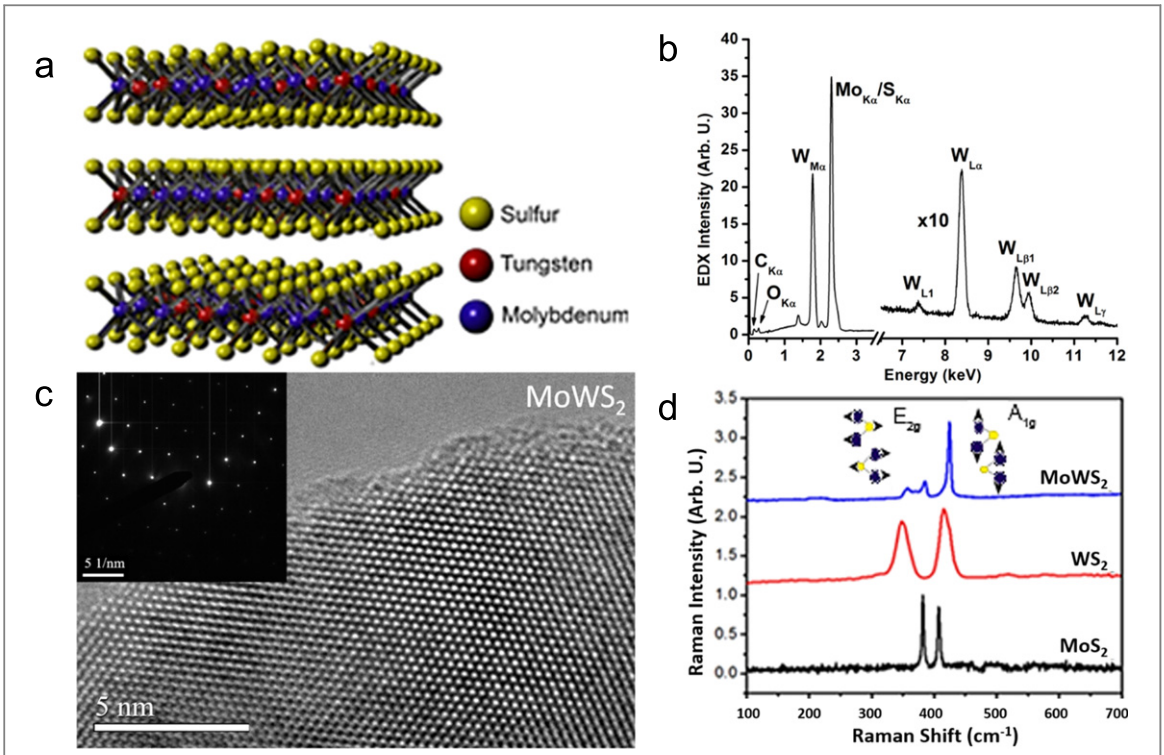

Figure 1. Characterization of structural and vibrational properties of $Mo_{0.5}W_{0.5}S_2$ ternary compound at ambient conditions. (a) A rendering depicting the ternary compound $Mo_{0.5}W_{0.5}S_2$ layered structure. Tungsten and molybdenum atoms are randomly distributed. (b) SEM–EDX spectrum showing fluorescence characteristics of Mo, W, and S elements. The peaks at energy range of 7–12 keV associated with the W fluorescence signals are enlarged. (c) TEM image of a $Mo_{0.5}W_{0.5}S_2$ thin film showing the layered pattern of the material. The inset shows the selected area electron diffraction (SAED) pattern exhibiting the diffraction pattern of the $Mo_{0.5}W_{0.5}S_2$ compound. The brighter spots correspond to the reflection of the W and Mo atoms in the lattice, although they are indistinguishable in the pattern. The sulfur atoms are not resolved. (d) Comparison of the Raman spectra of WS_2, MoS_2 and $Mo_{0.5}W_{0.5}S_2$ compound at ambient conditions. $Mo_{0.5}W_{0.5}S_2$ compound has a convolution of the Raman bands observed in the MoS_2 and WS_2 materials. The inset shows the lattice movements for the E_{2g} and A_{1g} Raman vibrational modes. MoS_2 and WS_2 samples used for comparison were purchased from SPI supplies and 2D semiconductors, respectively.

superimposed at wavenumber 420–430 cm^{-1}. Further analysis of the Raman spectrum of the $Mo_{0.5}W_{0.5}S_2$ compound studied here shows additional hybridized Raman peaks that are not present in the individual MoS_2 and WS_2 compounds at ambient conditions (figure 1(d)).

Using a DAC, hydrostatic pressure can be applied to the material which causes compression along all directions (both *c-axis* and *a-axis*), allowing for in-plane and out-of-plane strains to be studied [34, 48, 49]. Due to the anisotropic nature of the vdW compounds, it is expected that applied pressure will result in more significant compression in the out-of-plane direction than in the in-plane direction. Previous high pressure studies on multilayered MoS_2 and WS_2 clearly demonstrated that a metallization transition arises from strong interlayer interactions between S–S atoms due to the shortened interlayer distance at applied pressures [35, 36, 50]. Studying the *in situ* change in the hybridized A_{1g} and E_{2g} modes with hydrostatic pressure has been shown to be useful in deciphering the electronic isostructural phase transitions and the disorder-activated phonon behavior [34, 36]. In our study on the ternary compound here, both the E_{2g} and the A_{1g} modes from the MoS_2 and WS_2 are convoluted in the $Mo_{0.5}W_{0.5}S_2$ compound (figure 2(a)). The prominence of the A_{1g} mode is significant in comparison to the E_{2g} modes since the A_{1g} modes for the MoS_2 and WS_2 are separated only by $\Delta \approx 8\ cm^{-1}$, while the E_{2g} modes are further separated at $\Delta \approx 34\ cm^{-1}$. The asymmetric shape of the A_{1g} peak, with a shoulder on lower-wavenumber side, also implies that the two A_{1g} peaks are superimposed within the prominent peak. Note that a small peak at $\sim$370 cm^{-1} at 2.3 GPa between the two E_{2g} modes corresponds to the disorder-activated longitudinal acoustic (DALA) phonon mode [22–24], that represents the nature of the lattice disorder in the ternary compound. Further analysis of the measured Raman spectra using the Lorentzian curve fitting shows this peak to be prominent up to >35 GPa (figure S3).

Further increasing the pressure on the material, a peak, namely A^* emerged at $\sim$8 GPa (near the A_{1g} peaks) and continued to grow in intensity (figures 2(a) and (b)). The fact that neither MoS_2 nor WS_2 have been reported to has a new peak develop at $\sim$470 cm^{-1} at such a pressure range suggests that the A^* peak is related to disorder of the metal atoms at pressures. Moreover, pressure-related activation and enhancement of the peak further implies that its origin is related to the disorder-activated out-of-plane vibration mode. Increasing hydrostatic pressure is expected to

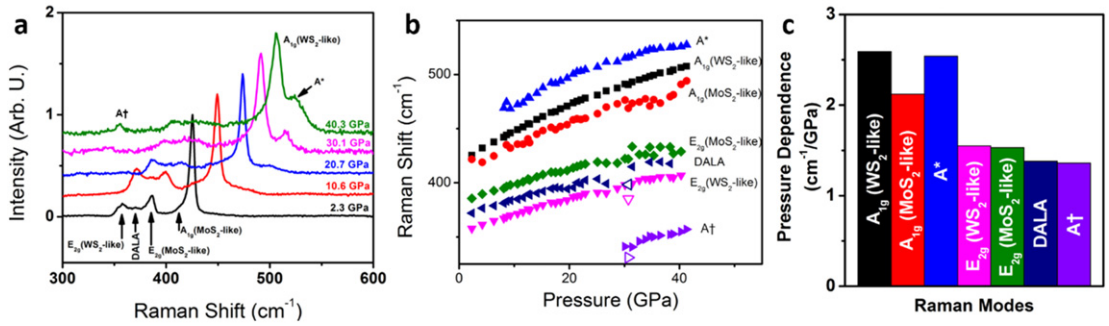

Figure 2. Evolution of Raman bands of $Mo_{0.5}W_{0.5}S_2$ compound under high pressure. (a) Representative Raman spectra with increasing pressure. Most Raman bands exhibit blue-shift (phonon hardening) as a function of pressure. Appearance of A^* and A† peaks are observed at high pressures. (b) The evolution of the Raman frequency shifts reveals the comprehensive pressure-effect on $Mo_{0.5}W_{0.5}S_2$. The two A_{1g} peaks and two E_{2g} peaks, as well as disorder-activated longitudinal acoustic (DALA) peak experience blue-shift with increasing pressure. The appearance of the A^* and A† peaks, first observed at ~8 GPa and ~30 GPa, respectively, suggest increasing disorder of the lattice. The A†, WS_2-like E_{2g}, and DALA peaks at pressure 30.7 GPa are marked as open symbols to note its deviation toward lower wavenumber. (c) Pressure dependent Raman coefficient of the vibrational peaks using the linear-fitting to the Raman shifts as a function of pressure. A_{1g} peaks and A^* peak show high pressure dependence compared to E_{2g} peaks and A† peak.

decrease the inter-layer distance of the multi-layer $Mo_{0.5}W_{0.5}S_2$, and therefore would increase the interaction between neighboring layers, which have a non-uniform distribution of Mo and W metal atoms along the *c-axis*. It is worthwhile to make a comparison with the DALA, which is related to in-plane metal–metal disorder and therefore observed even without external pressure. Pressure dependence of A^* peak similar to that of A_{1g} peaks further supports that the peak originated from the out-of-plane disorder, rather than the in-plane vibration (figure 2(c)). The E_{2g} modes and DALA mode stay convoluted to form a plateau near 350–400 cm^{-1}, which evolved together to higher wavenumber with increasing pressure (figures 2(a), and S4). Preserved shape of the plateau suggests the DALA mode survives up to higher pressure.

At ~30 GPa, another peak (denoted here as A†) was observed at 350 cm^{-1} suggesting that the $Mo_{0.5}W_{0.5}S_2$ compound has further developed an additional disorder-activated vibrational mode at this pressure (figure 2(b)). The A† peak continued to evolve to higher wavenumber at a rate of approximately 1.4 cm^{-1} GPa^{-1} that is higher compared to neighboring E_{2g} modes or DALA peak, but is rather closer to that of A_{1g} modes or A^* peak (figures 2(b) and (c)). This higher pressure dependence suggests that A† peak has closer lattice movement to A^* peak rather than DALA peak. Therefore the origin of A† peak could be speculated as another form of the disorder-activated vibrational mode [23, 24, 40]. However, we note that other explanation for the origin of A† peak may be possible. For example, considering the wavenumber and pressure dependence of A†, E_{1g} modes at 286 cm^{-1} (MoS_2) and 305 cm^{-1} (WS_2) observed under certain polarization [51–53] could be activated by lattice distortion. Further experiments involving infrared, absorption spectroscopy, and x-ray diffraction (XRD) as well as theoretical calculation are needed to fully understand the origin of the A† peak. Note that at 30.7 GPa, A† peak and E_{2g} peaks are at slightly lower wavenumber and the intensity of A† is significantly larger compared to other pressures (open symbols in figures 2(b), and S4 and S5). Other than the A† and E_{2g} peaks, however, other Raman peaks are not affected. We speculate that this phenomenon is correlated to lattice sliding like those observed in other TMD materials [35, 48, 54, 55].

To further confirm the phonon evolution and its origin, the Raman shifts of the $Mo_{0.5}W_{0.5}S_2$ compound are compared with Raman shifts of pristine MoS_2 and WS_2 at high pressures [34, 35, 50]. The Raman frequencies of both A_{1g} modes of $Mo_{0.5}W_{0.5}S_2$ as a function of pressure are in good agreement with that of the A_{1g} modes of MoS_2 and WS_2 (figure 3(a)). WS_2-like A_{1g} mode showed similar behavior to the A_{1g} mode in WS_2. MoS_2-like A_{1g} mode, on the other hand, shows no phonon softening at 10–20 GPa where pure MoS_2 experiences phonon softening during metallization [35]. Slight softening of phonon was observed at rather higher pressure of 25–35 GPa (figure 3(a)), speculating possible isostructural phase transition or metallization similar to those of MoS_2 end member, which requires further electrical conductivity measurements to confirm. The attenuated phonon softening might be attributed to the random distribution of Mo/W atoms, or effect of localized metallization centered at Mo atom sites. The in-plane Raman mode comparison also provided a fairly good match between $Mo_{0.5}W_{0.5}S_2$, MoS_2, and WS_2 (figure 3(b)), but with some blue-shift in case of $Mo_{0.5}W_{0.5}S_2$. These comparisons suggest that out-of-plane vibration modes (A_{1g}) are less affected by the disorder, due to the chalcogen-sandwich structure screening effects of disorder in metal atoms. Note that the pressure dependence of the MoS_2 and WS_2 compounds is adopted from previous work [35, 50].

Studying the full-width-half-maximum (FWHM) change with pressure can clarify electronic changes in

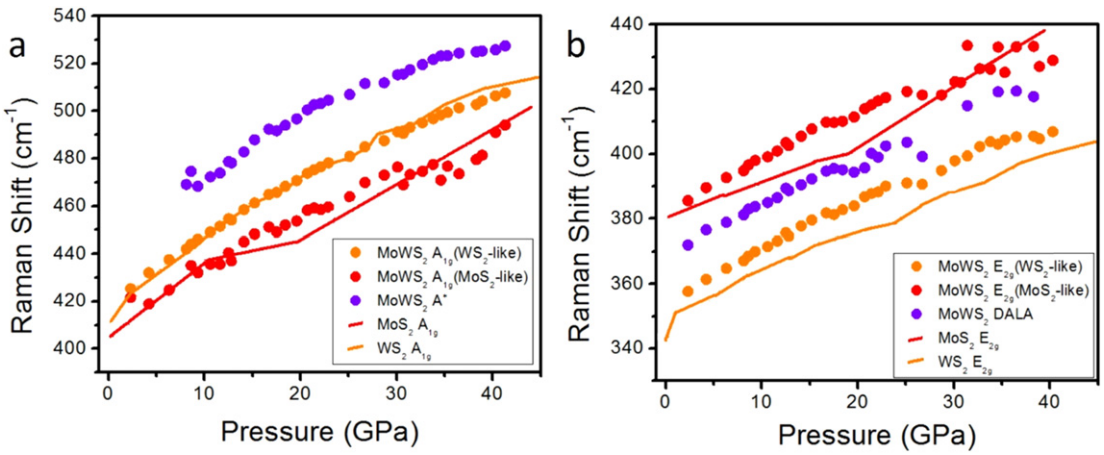

Figure 3. Comparison of Raman shifts of MoS_2, WS_2, and $Mo_{0.5}W_{0.5}S_2$ compound as a function of pressure. The pressure dependence of the out-of-plane A_{1g} phonon modes (a) and the in-plane E_{2g} phonon modes (b) of the ternary compound were compared with that of pristine WS_2 and MoS_2. Overall trends of the Raman shifts of the ternary compound are in good agreement with the pristine materials, but the E_{2g} modes show relatively less agreement compared to the A_{1g} modes suggesting a stronger effect of disorder.

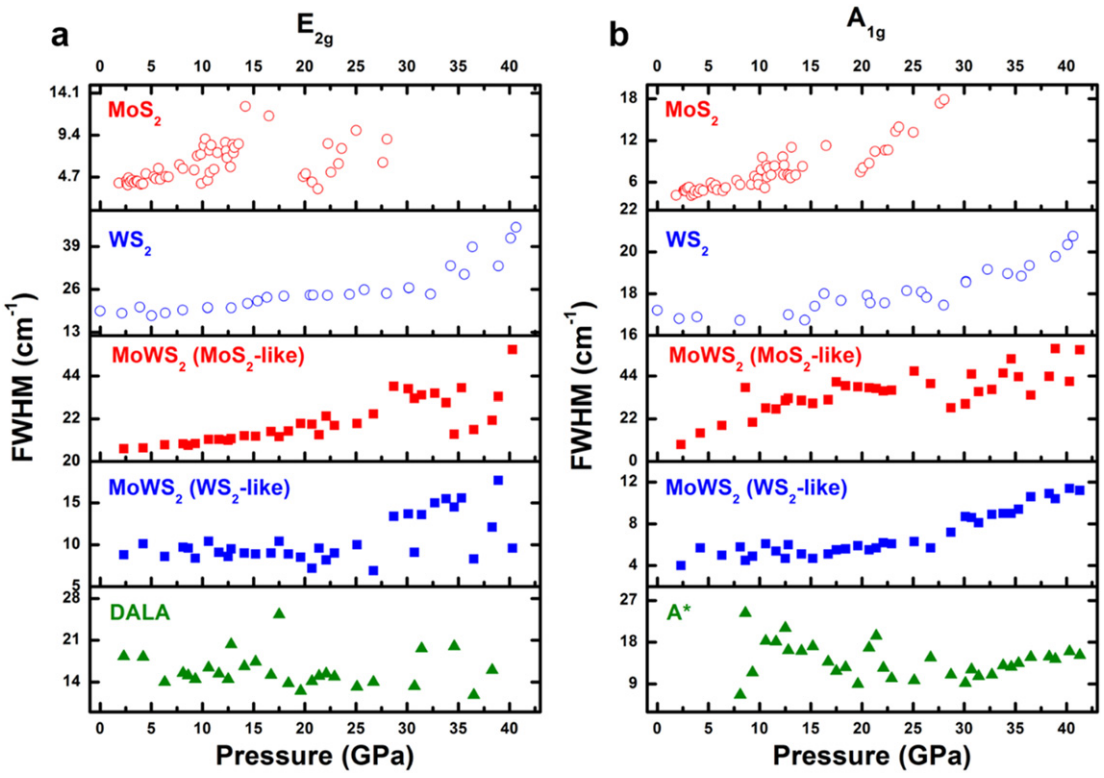

Figure 4. Pressure-dependent full-width half-maximum (FWHM) of Raman peaks for MoS_2, WS_2, and $Mo_{0.5}W_{0.5}S_2$ ternary compound. FWHM of (a) in-plane E_{2g} modes and (b) out-of-plane A_{1g} modes from MoS_2, WS_2, and $Mo_{0.5}W_{0.5}S_2$ was compared to further understand the pressure dependence of each phonon mode. The E_{2g} and A_{1g} modes of $Mo_{0.5}W_{0.5}S_2$ experienced an increase of FWHM with pressure, with the exception of the MoS_2-like E_{2g} mode which shows an undefined dependence at approximately 30 GPa. The FWHM of the DALA and A^* modes did not appear to show any consistent pressure-induced changes.

the material (figure 4) [35, 56]. In the MoS_2, FWHM of both the E_{2g} and A_{1g} peak slowly increase up to ~17 GPa where a significant drop is observed; this implies isostructural phase transition and metallization. For the $Mo_{0.5}W_{0.5}S_2$ compound, the FWHM of the peaks monotonically increases without any abrupt drop up to ~40 GPa. Absence of such FWHM decrease may be attributed to suppression of isostructural phase transition due to metal–metal disorder. The behavior of the DALA peak and the A^* peak are quite different compared to E_{2g} and A_{1g} peaks. DALA peak FWHM is not significantly affected by pressure. A^* peak FWHM decreased from its first observation at ~8 GPa through ~30 GPa. The decrease of FWHM supports that the A^* mode activates and develops into an explicit phonon mode as pressure increases and

thus inter-layer distance decreases. After 30 GPa, the A^* peak also widens due to pressure effect. The shift in the FWHM could suggest Davydov splitting observed in GaSe [57], GaS [58], as well as MoS_2 [59]. The effects of pressure on increasing the FWHM can be visualized in figure S4.

4. Conclusion

Hydrostatic pressure up to 40 GPa was applied to $Mo_{0.5}W_{0.5}S_2$ layered ternary compound to study the vibrational modes and understand the phonon and lattice distortion for high compressive forces. Our high pressure results show that with increasing pressure, the in-plane E_{2g} modes and out-of-plane A_{1g} modes follow closely to that of pristine MoS_2 or WS_2. MoS_2-like A_{1g} peak experiences slight phonon softening at 25–35 GPa, where pure MoS_2 experiences at 10–20 GPa with metallization. A peak (denoted A^*) enhances as pressure increases to ~8 GPa, with similar pressure dependence to A_{1g} modes. The FWHM of the A^* peak showed no notable increase as increasing pressure, suggesting that this peak originates from the out-of-plane disorder of metal atoms. Another new peak (denoted A†) first observed at ~30 GPa, could signify a further developing disorder in the lattice. To fully comprehend the origin of newly reported A† peak, as well as phonon softening of MoS_2-like A_{1g} mode, future study of the crystal structure using XRD, and electrical conductivity measurements will be of vital importance.

Acknowledgments

Research at The University of Texas at Austin was supported in part by a Young Investigator Award (DA) from the Defense Threat Reduction Agency (DTRA). SP, IR, GP, DR, and JH acknowledges support from the Young Scholars program of the NASCENT Engineering Research Center (Cooperative Agreement No. EEC-1160494). JFL acknowledges the support of NSAF (Grant No: U1530402). We also thank Tianshu Li for his thoughtful discussions, and Jo Wozniak for her contribution to figure illustrations.

References

[1] Geim A K and Novoselov K S 2007 The rise of graphene *Nat. Mater.* **6** 183–91
[2] Meric I *et al* 2013 Graphene field-effect transistors based on boron–nitride dielectrics *Proc. IEEE* **101** 1609–19
[3] Lee J *et al* 2013 High-performance current saturating graphene field-effect transistor with hexagonal boron nitride dielectric on flexible polymeric substrates *IEEE Electron Device Lett.* **34** 172–4
[4] Wang Q H, Kalantar-Zadeh K, Kis A, Coleman J N and Strano M S 2012 Electronics and optoelectronics of two-dimensional transition metal dichalcogenides *Nat. Nano* **7** 699–712
[5] Tao L *et al* 2015 Silicene field-effect transistors operating at room temperature *Nat. Nano* **10** 227–31
[6] Li L *et al* 2014 Black phosphorus field-effect transistors *Nat. Nano* **9** 372–7
[7] Akinwande D, Petrone N and Hone J 2014 Two-dimensional flexible nanoelectronics *Nat. Commun.* **5** 5678
[8] Chen Y *et al* 2013 Tunable band gap photoluminescence from atomically thin transition-metal dichalcogenide alloys *ACS Nano* **7** 4610–6
[9] Berkdemir A *et al* 2013 Identification of individual and few layers of WS_2 using Raman spectroscopy *Sci. Rep.* **3** 1755
[10] Ganatra R and Zhang Q 2014 Few-layer MoS_2: a promising layered semiconductor *ACS Nano* **8** 4074–99
[11] Splendiani A *et al* 2010 Emerging photoluminescence in monolayer MoS_2 *Nano Lett.* **10** 1271–5
[12] Dresselhaus M S 1987 Intercalation in layered materials *MRS Bull.* **12** 24–8
[13] Mahler B, Hoepfner V, Liao K and Ozin G A 2014 Colloidal synthesis of 1T-WS2 and 2H-WS2 nanosheets: applications for photocatalytic hydrogen evolution *J. Am. Chem. Soc.* **136** 14121–7
[14] Ohuchi F S, Jaegermann W, Pettenkofer C and Parkinson B A 1989 Semiconductor to metal transition of WS_2 induced by K intercalation in ultrahigh vacuum *Langmuir* **5** 439–42
[15] Ni Z H *et al* 2008 Uniaxial strain on graphene: Raman spectroscopy study and band-gap opening *ACS Nano* **2** 2301–5
[16] Conley H J *et al* 2013 Bandgap engineering of strained monolayer and bilayer MoS_2 *Nano Lett.* **13** 3626–30
[17] Geim A K and Grigorieva I V 2013 Van der Waals heterostructures *Nature* **499** 419–25
[18] Duesberg G S 2014 Heterojunctions in 2D semiconductors: a perfect match *Nat. Mater.* **13** 1075–6
[19] Gong Y *et al* 2014 Vertical and in-plane heterostructures from WS_2/MoS_2 monolayers *Nat. Mater.* **13** 1135–42
[20] Ci L *et al* 2010 Atomic layers of hybridized boron nitride and graphene domains *Nat. Mater.* **9** 430–5
[21] Srivastava S K, Mandal T K and Samantaray B K 1997 Studies on layer disorder, microstructural parameters and other properties of tungsten-substitued molybdenum disulfide, $Mo_{1-x}W_xS_2$ ($0 \leqslant x \leqslant 1$) *Synth. Met.* **90** 135–42
[22] Qiao X-F *et al* 2015 Substrate-free layer-number identification of two-dimensional materials: a case of $Mo_{0.5}W_{0.5}S_2$ alloy *Appl. Phys. Lett.* **106** 223102
[23] Chen Y *et al* 2014 Composition-dependent Raman modes of $Mo_{1-x}W_xS_2$ monolayer alloys *Nanoscale* **6** 2833–9
[24] Dumcenco D O, Chen K Y, Wang Y P, Huang Y S and Tiong K K 2010 Raman study of 2H-$Mo_{1-x}W_xS_2$ layered mixed crystals *J. Alloys Compd.* **506** 940–3
[25] Huang X *et al* 2013 Solution-phase epitaxial growth of noble metal nanostructures on dispersible single-layer molybdenum disulfide nanosheets *Nat. Commun.* **4** 1444
[26] Song J-G *et al* 2015 Controllable synthesis of molybdenum tungsten disulfide alloy for vertically composition-controlled multilayer (S) *Nat. Commun.* **6** 1–17
[27] Lin Z *et al* 2014 Facile synthesis of MoS_2 and $Mo_xW_{1-x}S_2$ triangular monolayers *APL Mater.* **2** 092804
[28] Elías A L *et al* 2013 Controlled synthesis and transfer of large-area WS_2 sheets: from single layer to few layers *ACS Nano* **7** 5235–42
[29] Xi J, Zhao T, Wang D and Shuai Z 2014 Tunable electronic properties of two-dimensional transition metal dichalcogenide alloys: a first-principles prediction *J. Phys. Chem. Lett.* **5** 285–91
[30] Wang L, Sofer Z, Luxa J and Pumera M 2015 $Mo_xW_{1-x}S_2$ solid solutions as 3D electrodes for hydrogen evolution reaction *Adv. Mater. Interfaces* **2** 1500041
[31] Chandrasekar H and Nath D N 2015 Electron mobility in few-layer $Mo_xW_{1-x}S_2$ *Mater. Res. Express* **2** 095007
[32] Amin B, Kaloni T P and Schwingenschlogl U 2014 Strain engineering of WS_2, WSe_2, and WTe_2 *RSC Adv.* **4** 34561–5
[33] He K, Poole C, Mak K F and Shan J 2013 Experimental demonstration of continuous electronic structure tuning via strain in atomically thin MoS_2 *Nano Lett.* **13** 2931–6
[34] Nayak A P *et al* 2014 Pressure-dependent optical and vibrational properties of monolayer molybdenum disulfide *Nano Lett.* **15** 346–53

[35] Nayak A P et al 2014 Pressure-induced semiconducting to metallic transition in multilayered molybdenum disulphide Nat. Commun. 5 3731
[36] Zhao Z et al 2015 Pressure induced metallization with absence of structural transition in layered molybdenum diselenide Nat. Commun. 6 7312
[37] Voiry D et al 2013 Enhanced catalytic activity in strained chemically exfoliated WS_2 nanosheets for hydrogen evolution Nat. Mater. 12 850–5
[38] Eda G et al 2011 Photoluminescence from chemically exfoliated MoS_2 Nano Lett. 11 5111–6
[39] Mouri S, Miyauchi Y and Matsuda K 2013 Tunable photoluminescence of monolayer MoS_2 via chemical doping Nano Lett. 13 5944–8
[40] Zhang X et al 2015 Phonon and Raman scattering of two-dimensional transition metal dichalcogenides from monolayer, multilayer to bulk material Chem. Soc. Rev. 44 2757–85
[41] Ferrari A C and Basko D M 2013 Raman spectroscopy as a versatile tool for studying the properties of graphene Nat. Nano 8 235–46
[42] Georgakilas V et al 2012 Functionalization of graphene: covalent and non-covalent approaches, derivatives and applications Chem. Rev. 112 6156–214
[43] Martins Ferreira E H et al 2010 Evolution of the Raman spectra from single-, few-, and many-layer graphene with increasing disorder Phys. Rev. B 82 125429
[44] Najmaei S et al 2014 Tailoring the physical properties of molybdenum disulfide monolayers by control of interfacial chemistry Nano Lett. 14 1354–61
[45] Zhao Y et al 2013 Interlayer breathing and shear modes in few-trilayer MoS_2 and WSe_2 Nano Lett. 13 1007–15
[46] Gaur A P S, Sahoo S, Scott J F and Katiyar R S 2015 Electron–phonon interaction and double-resonance Raman studies in monolayer WS_2 J. Phys. Chem. C 119 5146–51
[47] Livneh T and Spanier J E 2015 A comprehensive multiphonon spectral analysis in MoS_2 2D Mater. 2 035003
[48] Hromadová L, Martoňák R and Tosatti E 2013 Structure change, layer sliding, and metallization in high-pressure MoS_2 Phys. Rev. B 87 144105
[49] Bandaru N et al 2014 Structural stability of WS_2 under high pressure Int. J. Mod. Phys. B 28 1450168
[50] Nayak A P et al 2015 Pressure-modulated conductivity, carrier density, and mobility of multilayered tungsten disulfide ACS Nano 9 9117–23
[51] Dumcenco D O et al 2011 Polarization dependent Raman active modes study of the $Mo_{1-x}W_xS_2$ mixed layered crystals Chin. J. Phys. 49 270–7
[52] Rice C et al 2013 Raman-scattering measurements and first-principles calculations of strain-induced phonon shifts in monolayer MoS_2 Phys. Rev. B 87 081307
[53] Terrones H et al 2014 New first order Raman-active modes in few layered transition metal dichalcogenides Sci. Rep. 4 4215–4215
[54] Guo H, Yang T, Tao P, Wang Y and Zhang Z 2013 High pressure effect on structure, electronic structure, and thermoelectric properties of MoS_2 J. Appl. Phys. 113 013709
[55] Livneh T and Sterer E 2010 Resonant Raman scattering at exciton states tuned by pressure and temperature in 2H-MoS_2 Phys. Rev. B 81 195209
[56] Bera A et al 2013 Sharp Raman anomalies and broken adiabaticity at a pressure induced transition from band to topological insulator in Sb_2Se_3 Phys. Rev. Lett. 110 107401
[57] Wieting T J and Verble J L 1972 Interlayer bonding and the lattice vibrations of β-GaSe Phys. Rev. B 5 1473–9
[58] Kuroda N and Nishina Y 1979 Davydov splitting of degenerate lattice modes in the layer compound GaS Phys. Rev. B 19 1312–5
[59] Molina-Sánchez A and Wirtz L 2011 Phonons in single-layer and few-layer MoS_2 and WS_2 Phys. Rev. B 84 155413

Supplementary Information

High Pressure Raman Study of Layered $Mo_{0.5}W_{0.5}S_2$ Ternary Compound

Joon-Seok Kim[1,*], Samuel T. Moran[1,2,*], Avinash P. Nayak[1,*], Shahar Pedahzur[2], Itzel Ruiz[2], Gabriela Ponce[2], Daniela Rodriguez[2], Joanna Henny[2], Jin Liu[3], Jung-Fu Lin[3,4,†] and Deji Akinwande[1,2,†]

[1] Department of Electrical and Computer Engineering, The University of Texas at Austin, Austin, Texas 78712, USA

[2] NASCENT NSF Engineering Research Center (ERC), Austin, Texas 78758, USA

[3] Department of Geological Sciences, The University of Texas at Austin, Austin, Texas 78712, USA

[4] Center for High Pressure Science & Technology Advanced Research (HPSTAR), Shanghai 201203, People's Republic of China

[*] These authors contributed equally to this work

[†] Corresponding authors

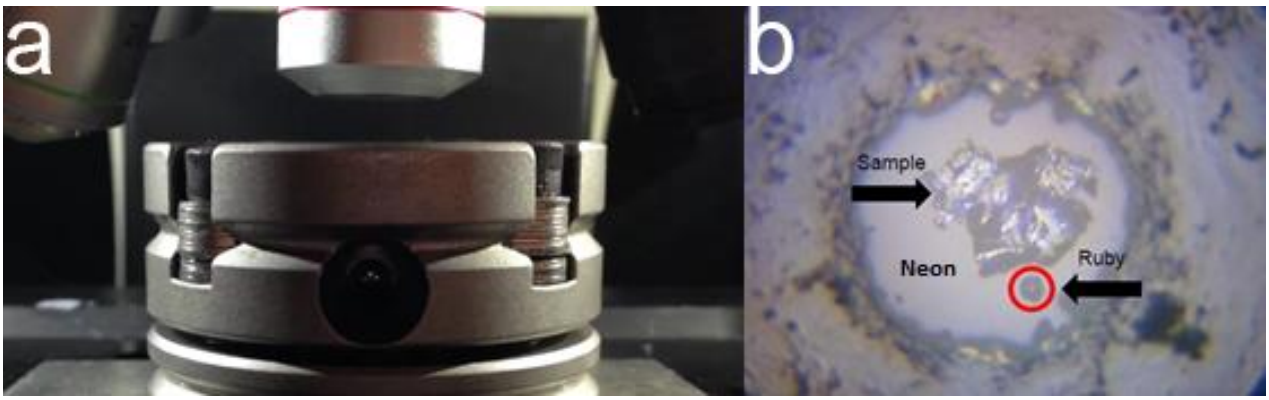

Figure S1. High-pressure Raman Experimental Setup Coupled with a DAC. (a) The DAC setup along with the laser Raman spectroscopy used for the Raman vibrational experiments. **(b)** A representative optical image of the sample chamber with the $Mo_{0.5}W_{0.5}S_2$ ternary compound, Ne pressure medium (transparent area), and a ruby pressure calibrant. A ruby sphere (red circle) is used to measure the pressure inside the sample chamber of the DAC.

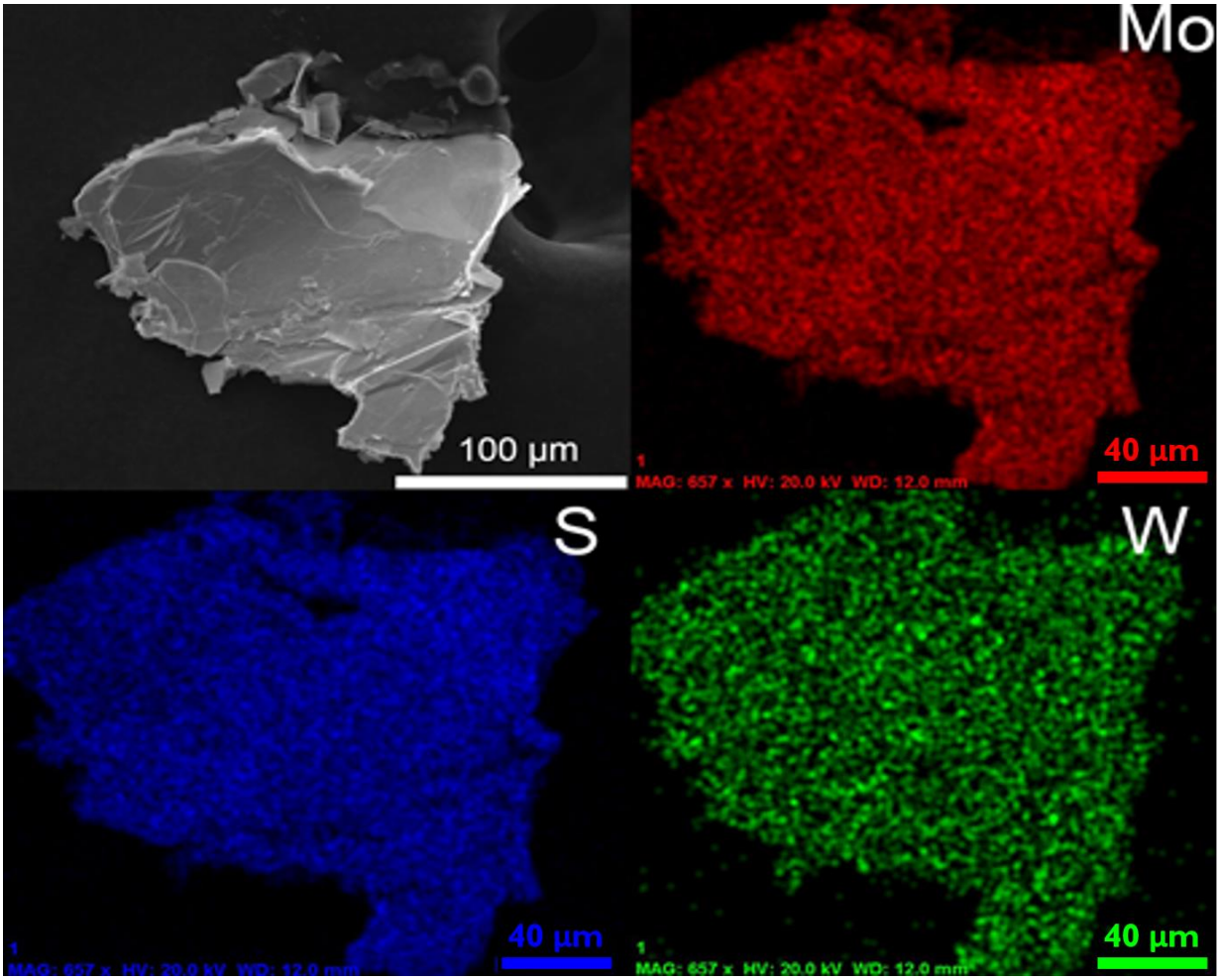

Figure S2. SEM-EDX Images of $Mo_{0.5}W_{0.5}S_2$ Ternary Compound. The energy dispersive x-ray spectroscopy (EDX) of a part of $Mo_{0.5}W_{0.5}S_2$ sample with molybdenum atoms indicated in red, sulfur atoms in blue, and tungsten atoms in green.

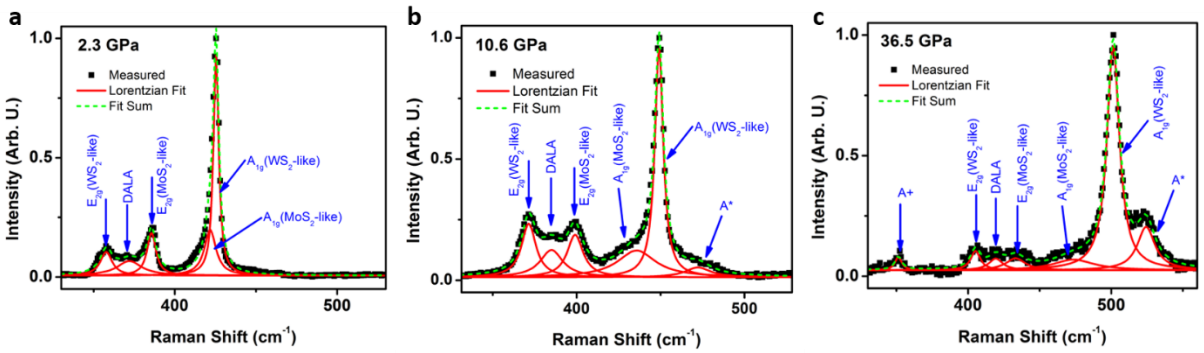

Figure S3. Lorentzian Fitting of Raman Spectra of $Mo_{0.5}W_{0.5}S_2$ Ternary Compound at High Pressure. Raman spectra, consisting of multiple Raman modes, were fitted using the Lorentzian curve fitting method. Representative Raman spectra at (**a**) 2.3 GPa, (**b**) 10.6 GPa with A* peak, and (**c**) 36.5 GPa with A† peak, are presented. Good fit of Lorentzian sum to the measured spectra suggests reliable representation of the fits to the evolution of the Raman peaks as a function of pressure.

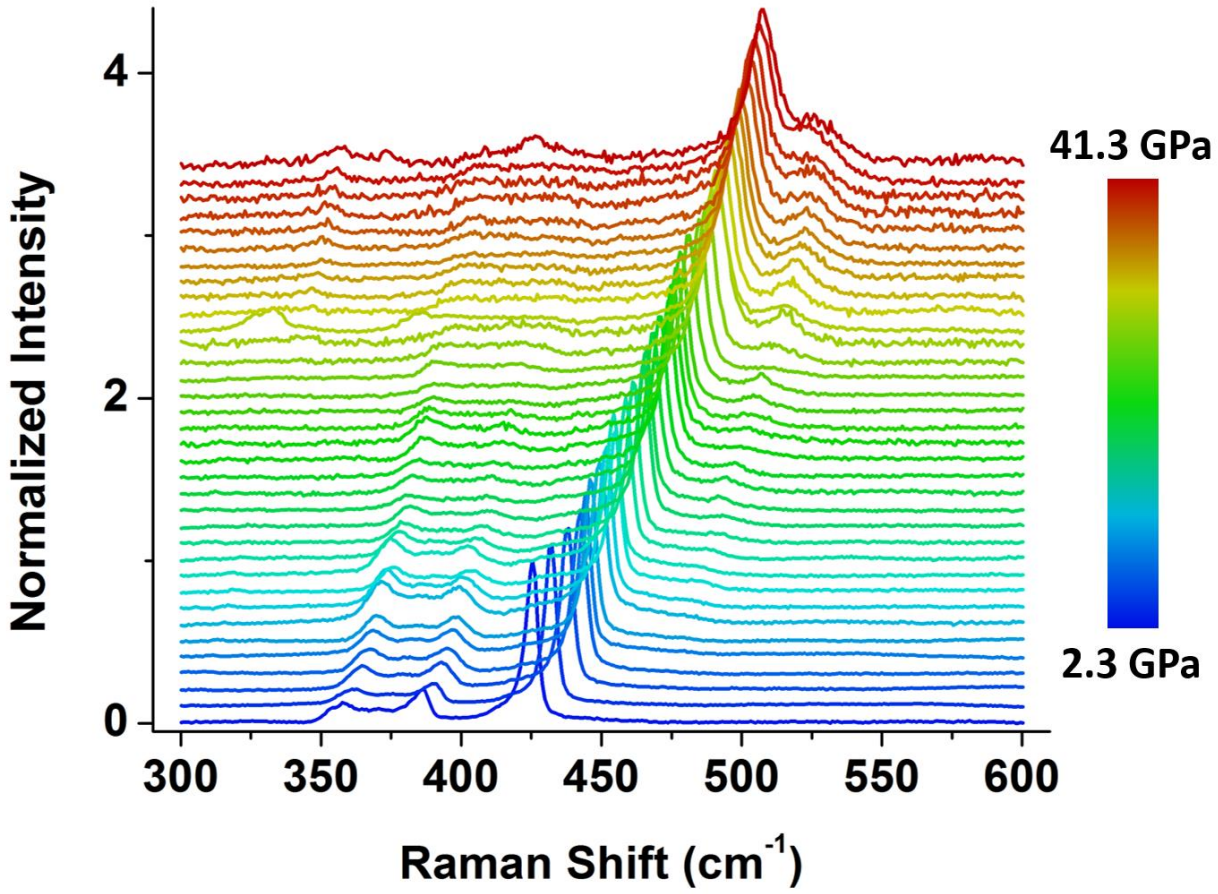

Figure S4. Evolution of Raman Spectra for $Mo_{0.5}W_{0.5}S_2$ Ternary Compound. Full stack of Raman spectra from 2.3 GPa (lowermost) to 41.3 GPa (uppermost), measured every 1-2 GPa in a diamond anvil cell. These spectra highlight the occurrence of the phonon hardening (blue-shift), and enhancement of the ternary compound at applied pressures.

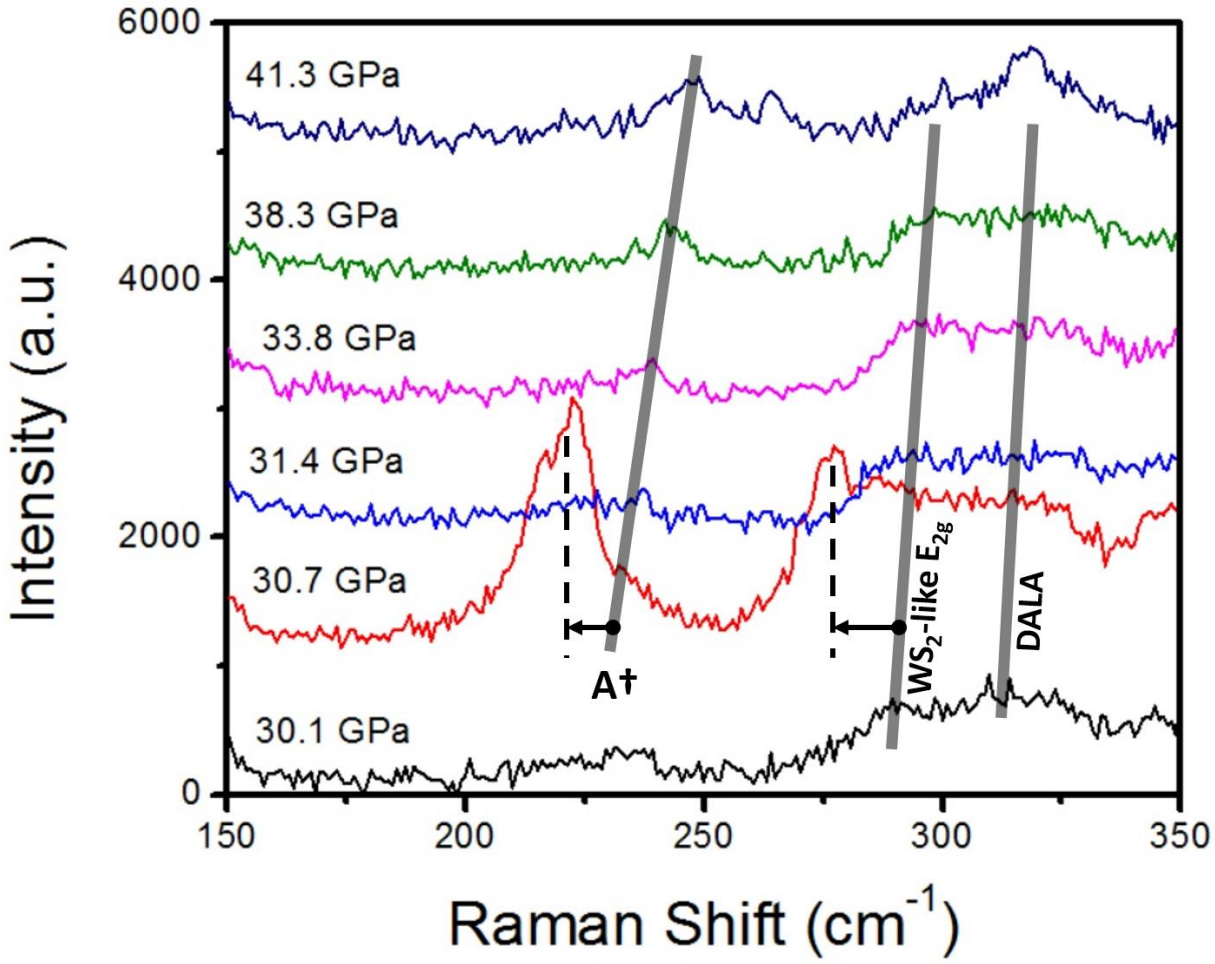

Figure S5. Representative Raman Spectra of the $Mo_{0.5}W_{0.5}S_2$ Ternary Compounds at Pressures Between 30 GPa and 41 GPa in the Lower Wavenumber Region. These spectra were collected using similar experimental conditions including laser power and collection time. At 30.7 GPa, WS_2-like E_{2g}, DALA, and developing A† peak experienced sudden deviation to lower wavenumber for ~10 cm^{-1}. Also, the intensity of A† peak is notably large at 30.7 GPa compared to any other pressures. This suggests potential lattice distortion at the pressure. However, thorough examination of structure is needed to fully understand the origin of this deviation and strong peak intensity.